Strong Coupling between Single Atoms and Nontransversal Photons

Christian Junge, Danny O'Shea, Jürgen Volz, and Arno Rauschenbeutel*

Vienna Center for Quantum Science and Technology, Atominstitut, Vienna University of Technology, 1020 Vienna, Austria

(Received 14 March 2013; published 22 May 2013)

Light is often described as a fully transverse-polarized wave, i.e., with an electric field vector that is orthogonal to the direction of propagation. However, light confined in dielectric structures such as optical waveguides or whispering-gallery-mode microresonators can have a strong longitudinal polarization component. Here, using single ^{85}Rb atoms strongly coupled to a whispering-gallery-mode microresonator, we experimentally and theoretically demonstrate that the presence of this longitudinal polarization fundamentally alters the interaction between light and matter.

DOI: 10.1103/PhysRevLett.110.213604 PACS numbers: 42.50.Pq, 42.25.Ja, 42.50.Ct, 42.60.Da

The interaction between light and matter basically underlies every optical process and application. For essentially plane waves in isotropic media, it has been quantitatively investigated in a number of ground-breaking experiments at the level of single atoms and single photons in high-finesse cavities [1–8]. In order to further enhance the light-matter coupling strength, an increasing number of recent experiments rely on waveguide structures [9–11] or high-numerical-aperture objectives [12–14]. However, in these situations, the physics changes drastically from the plane wave case because the polarization of the light fields is in general no longer transversal but exhibits a longitudinal component in the direction of propagation. This tags the propagation direction of the light by its polarization state and fundamentally renders full destructive interference of two counterpropagating waves impossible. One would thus expect this effect to have striking consequences for the physics of light-matter interaction.

Here, we quantitatively investigate this phenomenon in a model system consisting of single atoms that strongly interact with a whispering-gallery-mode (WGM) microresonator [15]. These resonators confine light by continuous total internal reflection and offer the advantage of very long photon lifetimes in conjunction with near-lossless in and out coupling of light via tapered fiber couplers [16]. As recently demonstrated in a series of pioneering experiments with toroidal WGM microresonators [17–22], single atoms as well as solid-state quantum emitters can be strongly coupled to WGMs. Beyond their importance in strong light-matter coupling, WGM microresonators are highly versatile photonic devices that have found applications in a large variety of disciplines. They have enabled, e.g., on-chip detection of single nanoparticles [23] and single viruses [24], the generation of optical frequency combs [25], as well as squeezed and correlated twin beams and single and pair photons [26,27]. Moreover, WGM microresonators provide a successful experimental platform in the thriving field of cavity optomechanics [28,29].

However, thus far, the nontransversal polarization of WGMs has not been taken into account in the description of the quantum mechanical interaction of light and matter. In particular, WGM microresonators were conceptually treated as conventional ring resonators that sustain a pair of degenerate, identically polarized, counterpropagating modes [17,19–23,30–35]. Under this assumption, the corresponding standing wave modes exhibit a full azimuthal intensity modulation with a phase that can be chosen such that one mode has a node at the position of a given emitter. As a consequence, this mode thus cannot interact with the atom, thereby leading to a fundamental limit of the performance of WGM microresonators for coupling light and matter. For instance, due to this uncoupled standing-wave mode, a single emitter should not be able to modify the on-resonant resonator transmission by more than 25% even with an arbitrarily large coupling strength [cf. Fig. 4(a)].

Here, we show that this picture is in general inadequate: In the case of nontransversally polarized WGMs, the two propagation directions of the photons are correlated with two nearly orthogonal polarization states. As a consequence, counterpropagating photons are distinguishable by their polarization and cannot interfere destructively, a situation not encountered in Fabry-Perot or conventional ring resonators. In particular, this effect prevents the formation of any uncoupled mode. In addition, the resonator field is almost perfectly circularly polarized in the plane of propagation despite the linear polarization of the pump light.

We investigate the consequences of this effect for light-matter coupling using WGM bottle microresonators [36–38], i.e., prolate-shaped cylindrically symmetric silica structures; see Fig. 1(a). These resonators sustain WGMs with ultrahigh quality factor ($Q \gtrsim 10^8$) and small mode volume, compatible with the requirements of cavity quantum electrodynamics in the strong coupling regime [37,38]. Compared to other types of ultrahigh-Q WGM microresonators, such as microspheres [39] and microtori [40], bottle microresonators have the additional advantage of being fully tunable [38]. Moreover, their mode geometry straightforwardly enables near-lossless simultaneous coupling of two independent tapered fiber couplers [41].

In order to model the interaction of single atoms with bottle microresonator modes (bottle modes), we employ

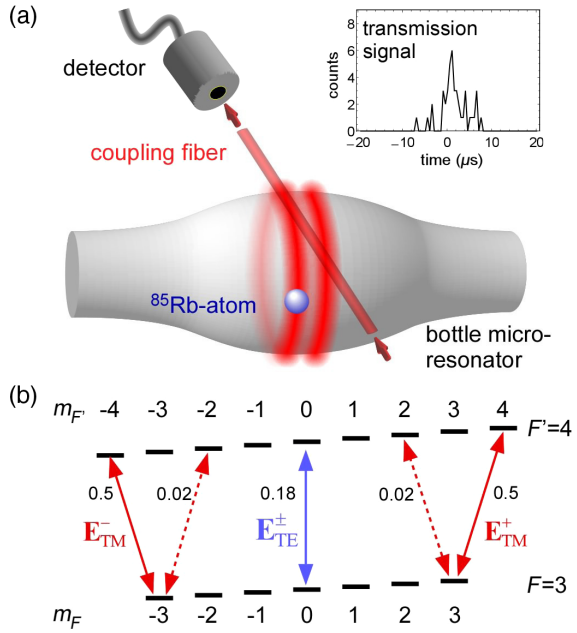

FIG. 1 (color online). (a) Schematic view of our bottle microresonator interfaced with a tapered fiber coupler. Probe light, launched into the coupling fiber, is coupled into the resonator via frustrated total internal reflection, and the remaining transmission is detected by a single photon counter. (b) Relevant atomic levels and transition strengths for ^{85}Rb. Because of the strong overlap with σ^+ (σ^-) polarization, TM modes drive $\Delta m_F = +1$ ($\Delta m_F = -1$) transitions, pumping into the Zeeman sublevel with maximum (minimum) m_F, while the π-polarized TE modes drive $\Delta m_F = 0$ transitions.

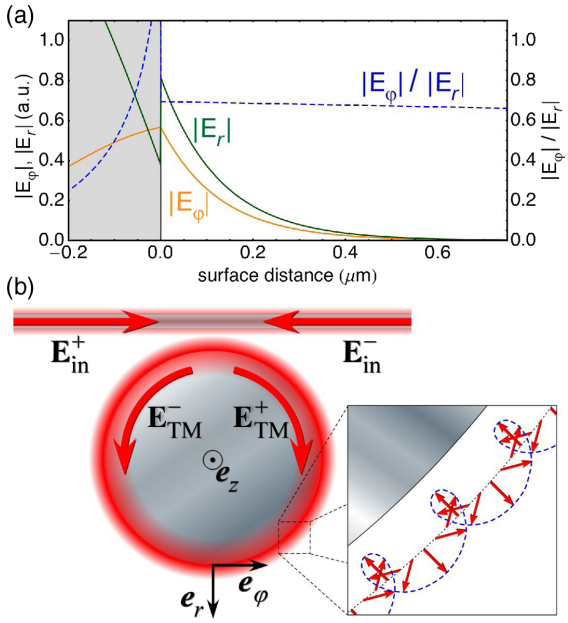

FIG. 2 (color online). (a) Longitudinal and transversal electric field components and their ratio as function of the distance to the resonator surface, calculated for the TM modes of our bottle microresonator. (b) In the case of TM modes, the spatial dependence of the electric field vector along the resonator is well described by a cycloid.

the Jaynes-Cummings Hamiltonian, generalized to a multilevel atom description and the full vectorial treatment of the evanescent electric field of a pair of counterpropagating bottle modes. As in all types of WGM microresonators, the light fields are guided by total internal reflection and the bottle modes can be classified according to the orientation of the electric field polarization, which either lies predominantly in the plane perpendicular to the resonator axis (TM) or predominantly points along this z axis (TE). TE modes are almost exclusively transversally polarized, i.e., their electric field vector is, to a good approximation, perpendicular to their wave vector at any position of the mode. In qualitative contrast, the TM modes are nontransversally polarized [42,43], meaning that the electric field vector of the evanescent field has a nonvanishing component along the wave vector; see Fig. 2(a). This longitudinal component oscillates $\pm 90°$ out of phase with respect to the transversal component. The $+$ ($-$) sign follows from Fresnel equations for the left-handed (right-handed) propagation sense of the mode with respect to the z axis, which defines our quantization axis. Thus, for a given distance from the resonator surface, the complex-valued amplitude vector of TM modes is

$$\mathbf{E}^{\pm}_{\mathrm{TM}} = \mathbf{E}_{\mathrm{trans}} \pm i\mathbf{E}_{\mathrm{long}}. \qquad (1)$$

Here, $\mathbf{E}_{\mathrm{trans}} \approx |\mathbf{E}_{\mathrm{trans}}|\mathbf{e}_r$ ($\mathbf{E}_{\mathrm{long}} = |\mathbf{E}_{\mathrm{long}}|\mathbf{e}_\varphi$) is the transversal (longitudinal) amplitude vector with the real-valued radial (azimuthal) unit vector $\mathbf{e}_r$ ($\mathbf{e}_\varphi$). The situation is much simpler for the TE modes, which have approximately the same amplitude vector for both rotation senses, $\mathbf{E}^{+}_{\mathrm{TE}} \approx \mathbf{E}^{-}_{\mathrm{TE}} \approx |\mathbf{E}^{\pm}_{\mathrm{TE}}|\mathbf{e}_z$, where $\mathbf{e}_z$ is the real-valued axial unit vector.

The sign in Eq. (1) has a decisive consequence for WGM resonators: For the sake of simplicity, let us first assume that $|\mathbf{E}_{\mathrm{trans}}| = |\mathbf{E}_{\mathrm{long}}|$. In this case, $\mathbf{E}^{+}_{\mathrm{TM}}$ and $\mathbf{E}^{-}_{\mathrm{TM}}$ describe two modes with mutually orthogonal circular polarizations. However, in contrast to what is usually encountered for freely propagating light fields, the plane of polarization is parallel to the local wave vector of the mode and the electric field vector describes a cycloid along the circumference of the resonator; see Fig. 2(b). Any superposition of such a pair of counterpropagating modes corresponds to a light field with azimuthally symmetric intensity and ellipticity. In other words, it is not possible to form an intensity-modulated standing wave in the resonator.

As a consequence, if an atom is coupled to any superposition of degenerate counterpropagating TM modes, the atom-light coupling strength is independent of the azimuthal position of the atom or, equivalently, of the relative phase of the superposition. In particular, this rules out the existence of an uncoupled standing wave mode with TM polarization. This differs fundamentally from what is encountered for standard paraxial Fabry-Perot and ring resonators, where this intrinsic connection between polarization and propagation direction does not occur.

For WGMs with maximal angular momentum, the ratio $|\mathbf{E}_{\text{long}}|/|\mathbf{E}_{\text{trans}}|$ is largely independent of the geometry and the diameter of the WGM resonator and almost exclusively determined by the refractive index of the resonator material (see Supplemental Material [44]). For WGM microresonators made of silica, one obtains $|\mathbf{E}_{\text{long}}|/|\mathbf{E}_{\text{trans}}| \approx 0.7$ [see Fig. 2(a)]. Thus, $|\mathbf{E}^{\pm}_{\text{TM}} \cdot \mathbf{e}^{*}_{\sigma^{\pm}}|^2/|\mathbf{E}^{\pm}_{\text{TM}}|^2 > 0.96$, where $\mathbf{e}_{\sigma^{\pm}} = (\mathbf{e}_r \pm i\mathbf{e}_\varphi)/\sqrt{2}$, meaning that $\mathbf{E}^{\pm}_{\text{TM}}$ modes almost fully overlap with an ideally circularly ($\sigma^{\pm}$) polarized mode. For higher refractive indices, the overlap will be even higher.

Besides preventing the formation of an uncoupled standing wave mode, the near perfect circular polarization of $\mathbf{E}^{\pm}_{\text{TM}}$ has an additional advantage: Consider the case where the resonator is, e.g., coupled to a single ^{85}Rb atom and light is launched into the coupling fiber in the direction of $\mathbf{E}^{+}_{\text{in}}$ in order to resonantly excite mode $\mathbf{E}^{+}_{\text{TM}}$; see Fig. 2(b). The atom then interacts with almost purely circularly polarized (σ^{+}) light, and transitions with $\Delta m_F = +1$ are predominantly driven, where m_F is the magnetic quantum number of the atomic hyperfine states. This leads to optical pumping and, when the $\mathbf{E}^{+}_{\text{TM}}$ mode is close to resonance with the atomic transition $5S_{1/2}$, $F = 3 \rightarrow 5P_{3/2}$, $F' = 4$, the atom is transferred to the outermost Zeeman sublevel with $F = 3$, $m_F = 3$ after a few scattering events; see Fig. 1(b). From there, light in the $\mathbf{E}^{+}_{\text{TM}}$ mode can only excite the $F' = 4$, $m_{F'} = 4$ state, which can only decay back to the $F = 3$, $m_F = 3$ ground state. This situation occurs naturally and is highly advantageous for two reasons: First, the closed cycling transition maximizes the coupling strength of the atom to the electromagnetic field. Second, the selection rules for dipole transitions prevent the atom from emitting light into the orthogonally polarized, counterpropagating $\mathbf{E}^{-}_{\text{TM}}$ mode. Despite the simultaneous existence of two degenerate resonator modes, this effectively leads to the ideal case of a two-level atom that only interacts with a single traveling-wave mode. Thus, our theoretical model predicts a spectrum of the coupled atom-resonator system that exhibits the well-known vacuum Rabi splitting of the resonance frequencies by $\Delta\omega = 2g$ [see Fig. 3(a)], where g is the atom-resonator coupling strength.

In the case of TE modes, both running waves have the same linear polarization. Thus, the atom will interact with both modes, and an uncoupled standing wave occurs. This leads to qualitatively different physical behavior compared to that of the TM case, which is apparent in the predicted spectrum, which contains an additional central resonance that is a signature of the uncoupled standing wave mode; see Fig. 4(a). This spectrum essentially corresponds to the predictions of the formerly employed theoretical model that neglected the nontransversal polarization of the resonator modes.

To verify that the above scenarios adequately describe our experiment, we investigate the physical behavior of TE and TM modes. Figure 1(a) shows a schematic of our experimental setup with the bottle microresonator

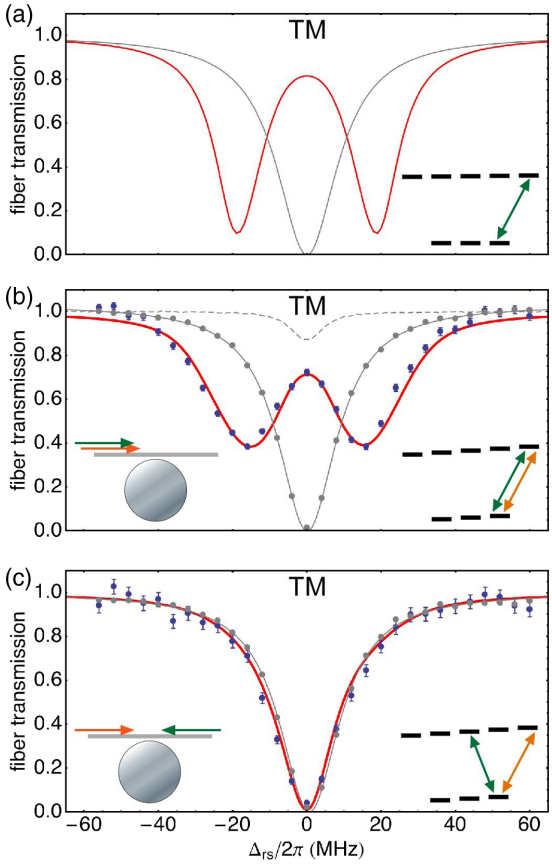

FIG. 3 (color online). (a) Calculated coupling fiber transmission for a TM mode coupled to a single atom with a fixed coupling strength of $g/2\pi = 20$ MHz and zero atom-resonator detuning (red line; see Supplemental Material [44]). The transmission for an empty resonator is shown by the gray line. (b) Measured fiber transmission for our TM mode (blue circles: experimental data; error bars indicate the 1σ statistical error) with a guiding field of $B_z = 4.5$ G. The red solid line is a theoretical fit yielding an average coupling strength of $\bar{g}/2\pi = 17$ MHz with a standard deviation of $\sigma_g/2\pi = 6$ MHz. The gray data show the transmission of the empty cavity with a Lorentzian fit yielding a HWHM of $\kappa/2\pi = 10$ MHz. The dashed line is the measured empty resonator transmission spectrum in the undercoupled regime. (c) Vacuum Rabi spectrum measured under same conditions as those in (b) but with application of the spectroscopy laser with a direction opposite to that of the detection laser. To avoid optical pumping by the spectroscopy laser, the spectrum is only measured for the first 100 ns. The theory curve is calculated using the same parameters $\bar{g}$ and σ_g as in (b). The insets show the direction of the detection (orange) and the spectroscopy light (green) and a simplified atomic level scheme indicating the driven transitions.

interfaced with a submicron diameter coupling fiber [45–47]. We tune the frequency of the bottle microresonator to the atomic $5S_{1/2}$, $F = 3 \rightarrow 5P_{3/2}$, $F' = 4$ transition of ^{85}Rb (transition wavelength $\lambda = 780$ nm) and critically couple the coupling fiber to the resonator. At this set point, the in- and out-coupling rate of light matches the intrinsic loss rate of the empty resonator. We set the polarization of the resonant light in the coupling fiber to match the

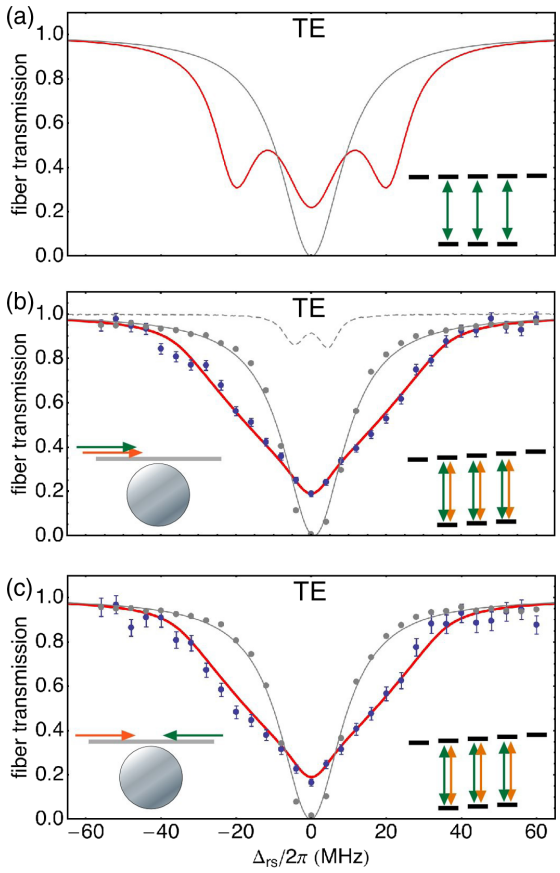

FIG. 4 (color online). (a–c) Same as Fig. 3 but for a TE-polarized mode. The fit in (b) yields an average coupling strength of $\bar{g}/2\pi = 17$ MHz with a standard deviation of $\sigma_g/2\pi = 9$ MHz.

polarization of the bottle mode. As a result, the light will be entirely coupled into the bottle microresonator mode and dissipated therein. The remaining transmission through the coupling fiber is typically as low as 1%; see Figs. 3 and 4. We then launch a cloud of laser-cooled ^{85}Rb atoms towards the resonator. If an atom enters the evanescent field of the resonator mode, the vacuum Rabi splitting of the resonance frequency of the strongly coupled atom-resonator system results in a significant increase of the coupling fiber transmission; see inset of Fig. 1(a). When such an event is registered, a fast optical switch is used to turn off the detection light in real time and to simultaneously apply a spectroscopy field through the coupling fiber that can be set to any relevant detuning $\Delta_{rs} = \omega_r - \omega_s$, where $\omega_r/2\pi$ and $\omega_s/2\pi$ are the frequencies of the resonator mode and spectroscopy field, respectively. See Supplemental Material [44] for further details.

Figures 3(b) and 4(b) show transmission spectra obtained for the case of probing a TM- and TE-polarized mode, $\mathbf{E}^{+}_{\mathrm{TM}}$ and $\mathbf{E}^{+}_{\mathrm{TE}}$, respectively. A guiding magnetic field $B_z = 4.5$ G along the z axis lifts the degeneracy of the Zeeman sublevels. The bottle resonator is set to resonance with the dominant atomic transition ($F = 3$, $m_F = 3 \rightarrow F' = 4$, $m'_F = 4$ for TM and $F = 3$, $m_F = 0 \rightarrow F' = 4$, $m'_F = 0$ for TE). Compared to the case of an atom-resonator system with a well-defined coupling constant g [Figs. 3(a) and 4(a)], in our experiment the coupling strength of the atoms varies, both during the transit and from shot to shot. We account for this by fitting an averaged spectrum to the transmission data, where the only free fit parameters are the mean value of the coupling strength $\bar{g}$ and its standard deviation σ_g. Perfect agreement is found between the experimental data and the theoretically predicted spectra. As expected, for the $\mathbf{E}^{+}_{\mathrm{TM}}$ mode, the spectrum clearly features two transmission dips whereas the spectrum for the $\mathbf{E}^{+}_{\mathrm{TE}}$ mode is dominated by a central dip.

We now launch the detection light along $\mathbf{E}^{+}_{\mathrm{in}}$ and the spectroscopy light along the opposite direction $\mathbf{E}^{-}_{\mathrm{in}}$. For the TE-polarized mode, we expect the same transmission spectrum as before. However, the situation is different for the TM modes, where we populate the $\mathbf{E}^{+}_{\mathrm{TM}}$ mode during detection and the atom is pumped into the $m_F = 3$ state. The spectroscopy is then carried out on the $\mathbf{E}^{-}_{\mathrm{TM}}$ mode, which initially drives the $F = 3$, $m_F = 3 \rightarrow F' = 4$, $m'_F = 2$ transition; see Fig. 1(b). This transition is strongly suppressed by two effects. First, its strength is more than 1 order of magnitude smaller than that for the closed cycling transition, and second, the strong interaction of the atom with the empty $\mathbf{E}^{+}_{\mathrm{TM}}$ mode on the $F = 3$, $m_F = 1 \rightarrow F' = 4$, $m'_F = 2$ transition leads to a vacuum Rabi splitting of the excited state. As a result, the transmission spectrum recorded with detection and spectroscopy light launched from opposite sides should initially closely resemble that of an empty resonator. Figures 3(c) and 4(c) show the transmission spectra of the TM and TE mode recorded for this case. The interaction time of the spectroscopy field with the coupled atom-resonator system was limited to the first 100 ns after the initial relaxation of the resonator field. We experimentally verified that this time interval is short enough to prevent optical depumping of the initial atomic state. The transmission spectrum predicted by our model in Figs. 3(c) and 4(c) [solid lines with the same values of $\bar{g}$ and σ_g as in Figs. 3(b) and 4(b)] shows excellent agreement between experiment and theory.

Summarizing, we experimentally and theoretically demonstrated that the longitudinal component of the electric field in whispering-gallery modes intrinsically correlates the polarization of counterpropagating photons in the resonator with their propagation direction. Beyond whispering-gallery-mode resonators, this effect inevitably occurs in all physical systems and situations that involve longitudinal polarization components. In particular, this includes optical waveguides, nanophotonic structures, and even focused beams that propagate in free space. The polarization-propagation correlation inhibits full destructive interference between counterpropagating photons and can thus qualitatively alter the resulting light field with respect to what is expected when treating light as fully transversal wave. In the case of WGM resonators, this phenomenon leads to a highly advantageous situation that allows one to

overcome the limitations of traditional ring resonators for coupling light and matter. In particular, it enables the control of the interaction between the atom and the two counterpropagating modes in the resonator. In combination with the demonstrated low optical losses of whispering-gallery-mode microresonators, this constitutes ideal conditions for the realization of photonic quantum devices in optical fiber-based networks.

We gratefully acknowledge financial support by the European Science Foundation, the Volkswagen Foundation, and the Austrian Science Fund (FWF; SFB FoQuS Project No. F 4017). J. V. acknowledges support by the European Commission (Marie Curie IEF Grant No. 300392). C. J. acknowledges support by the German National Academic Foundation.

*arno.rauschenbeutel@ati.ac.at

[1] K. M. Birnbaum, A. Boca, R. Miller, A. D. Boozer, T. E. Northup, and H. J. Kimble, Nature (London) **436**, 87 (2005).
[2] A. D. Boozer, A. Boca, R. Miller, T. E. Northup, and H. J. Kimble, Phys. Rev. Lett. **98**, 193601 (2007).
[3] T. Wilk, S. Webster, A. Kuhn, and G. Rempe, Science **317**, 488 (2007).
[4] M. L. Terraciano, R. O. Knell, D. G. Norris, J. Jing, A. Fernandez, and L. A. Orozco, Nat. Phys. **5**, 480 (2009).
[5] T. Kampschulte, W. Alt, S. Brakhane, M. Eckstein, R. Reimann, A. Widera, and D. Meschede, Phys. Rev. Lett. **105**, 153603 (2010).
[6] J. Volz, R. Gehr, G. Dubois, J. Esteve, and J. Reichel, Nature (London) **475**, 210 (2011).
[7] C. Sayrin, I. Dotsenko, X. Zhou, B. Peaudecerf, T. Rybarczyk, S. Gleyzes, P. Rouchon, M. Mirrahimi, H. Amini, M. Brune, J.-M. Raimond, and S. Haroche, Nature (London) **477**, 73 (2011).
[8] S. Ritter, C. Nolleke, C. Hahn, A. Reiserer, A. Neuzner, M. Uphoff, M. Mucke, E. Figueroa, J. Bochmann, and G. Rempe, Nature (London) **484**, 195 (2012).
[9] A. Stiebeiner, O. Rehband, R. Garcia-Fernandez, and A. Rauschenbeutel, Opt. Express **17**, 21 704 (2009).
[10] E. Vetsch, D. Reitz, G. Sagué, R. Schmidt, S. T. Dawkins, and A. Rauschenbeutel, Phys. Rev. Lett. **104**, 203603 (2010).
[11] J. Hwang and E. A. Hinds, New J. Phys. **13**, 085009 (2011).
[12] M. K. Tey, Z. Chen, S. A. Aljunid, B. Chng, F. Huber, G. Maslennikov, and C. Kurtsiefer, Nat. Phys. **4**, 924 (2008).
[13] K. G. Lee, X. W. Chen, H. Eghlidi, P. Kukura, R. Lettow, A. Renn, V. Sandoghdar, and S. Götzinger, Nat. Photonics **5**, 166 (2011).
[14] R. Maiwald, A. Golla, M. Fischer, M. Bader, S. Heugel, B. Chalopin, M. Sondermann, and G. Leuchs, Phys. Rev. A **86**, 043431 (2012).
[15] A. Matsko and V. Ilchenko, IEEE J. Sel. Top. Quantum Electron. **12**, 3 (2006).
[16] S. M. Spillane, T. J. Kippenberg, O. J. Painter, and K. J. Vahala, Phys. Rev. Lett. **91**, 043902 (2003).
[17] T. Aoki, B. Dayan, E. Wilcut, W. P. Bowen, A. S. Parkins, T. J. Kippenberg, K. J. Vahala, and H. J. Kimble, Nature (London) **443**, 671 (2006).
[18] Y. Park, A. Cook, and H. Wang, Nano Lett. **6**, 2075 (2006).
[19] K. Srinivasan and O. Painter, Nature (London) **450**, 862 (2007).
[20] B. Dayan, A. Parkins, T. Aoki, E. Ostby, K. Vahala, and H. Kimble, Science **319**, 1062 (2008).
[21] T. Aoki, A. S. Parkins, D. J. Alton, C. A. Regal, B. Dayan, E. Ostby, K. J. Vahala, and H. J. Kimble, Phys. Rev. Lett. **102**, 083601 (2009).
[22] D. J. Alton, N. P. Stern, T. Aoki, H. Lee, E. Ostby, K. J. Vahala, and H. J. Kimble, Nat. Phys. **7**, 159 (2010).
[23] J. Zhu, S. K. Ozdemir, Y.-F. Xiao, L. Li, L. He, D.-R. Chen, and L. Yang, Nat. Photonics **4**, 46 (2010).
[24] F. Vollmer, S. Arnold, and D. Keng, Proc. Natl. Acad. Sci. U.S.A. **105**, 20 701 (2008).
[25] P. Del'Haye, A. Schliesser, O. Arcizet, T. Wilken, R. Holzwarth, and T. J. Kippenberg, Nature (London) **450**, 1214 (2007).
[26] J. U. Fürst, D. V. Strekalov, D. Elser, A. Aiello, U. L. Andersen, C. Marquardt, and G. Leuchs, Phys. Rev. Lett. **106**, 113901 (2011).
[27] M. Förtsch, J. Fürst, C. Wittmann, D. Strekalov, A. Aiello, M. V. Chekhova, C. Silberhorn, G. Leuchs, and C. Marquardt, Nat. Commun. **4**, 1818 (2013).
[28] T. J. Kippenberg and K. J. Vahala, Science **321**, 1172 (2008).
[29] G. Bahl, M. Tomes, F. Marquardt, and T. Carmon, Nat. Phys. **8**, 203 (2012).
[30] L. He, S. K. Ozdemir, J. Zhu, W. Kim, and L. Yang, Nat. Nanotechnol. **6**, 428 (2011).
[31] P. Domokos, M. Gangl, and H. Ritsch, Opt. Commun. **185**, 115 (2000).
[32] M. Rosenblit, P. Horak, S. Helsby, and R. Folman, Phys. Rev. A **70**, 053808 (2004).
[33] K. Srinivasan and O. Painter, Phys. Rev. A **75**, 023814 (2007).
[34] J. T. Shen and S. Fan, Phys. Rev. A **79**, 023838 (2009).
[35] N. P. Stern, D. J. Alton, and H. J. Kimble, New J. Phys. **13**, 085004 (2011).
[36] M. Sumetsky, Opt. Lett. **29**, 8 (2004).
[37] Y. Louyer, D. Meschede, and A. Rauschenbeutel, Phys. Rev. A **72**, 031801 (2005).
[38] M. Pöllinger, D. O'Shea, F. Warken, and A. Rauschenbeutel, Phys. Rev. Lett. **103**, 053901 (2009).
[39] V. Braginsky, M. Gorodetsky, and V. Ilchenko, Phys. Lett. A **137**, 393 (1989).
[40] D. K. Armani, T. J. Kippenberg, S. M. Spillane, and K. J. Vahala, Nature (London) **421**, 925 (2003).
[41] M. Pöllinger and A. Rauschenbeutel, Opt. Express **18**, 17 764 (2010).
[42] D. Axelrod, T. Burghardt, and N. Thompson, Annu. Rev. Biophys. Bioeng. **13**, 247 (1984).
[43] T. Kawalec, L. Józefowski, J. Fiutowski, M. Kasprowicz, and T. Dohnalik, Opt. Commun. **274**, 341 (2007).
[44] See the Supplemental Material at http://link.aps.org/supplemental/10.1103/PhysRevLett.110.213604 for details on the polarization of the evanescent field, experimental techniques, and the modeling of the spectra.
[45] D. O'Shea, A. Rettenmaier, and A. Rauschenbeutel, Appl. Phys. B **99**, 623 (2010).
[46] D. O'Shea, C. Junge, M. Pöllinger, A. Vogler, and A. Rauschenbeutel, Appl. Phys. B **105**, 129 (2011).
[47] C. Junge, S. Nickel, D. O'Shea, and A. Rauschenbeutel, Opt. Lett. **36**, 3488 (2011).